Arg352 Is a Major Determinant of Charge Selectivity in the Cystic Fibrosis Transmembrane Conductance Regulator Chloride Channel †

ARTICLE *in* BIOCHEMISTRY · MAY 1999

Impact Factor: 3.02 · DOI: 10.1021/bi990155n · Source: PubMed

2 AUTHORS:

Romain Guinamard
Université de Caen Normandie
44 PUBLICATIONS **1,052** CITATIONS
SEE PROFILE

Myles H Akabas
Albert Einstein College of Medicine
93 PUBLICATIONS **6,253** CITATIONS
SEE PROFILE

Arg352 Is a Major Determinant of Charge Selectivity in the Cystic Fibrosis Transmembrane Conductance Regulator Chloride Channel†

Romain Guinamard‡ and Myles H. Akabas*,‡,§

Center for Molecular Recognition and Departments of Physiology & Cellular Biophysics and Medicine, Columbia University College of Physicians and Surgeons, 630 West 168th Street, New York, New York 10032

Received January 21, 1999; Revised Manuscript Received March 5, 1999

ABSTRACT: The cystic fibrosis transmembrane conductance regulator forms an anion-selective channel. We previously showed that charge selectivity, the ability to discriminate between anions and cations, occurs near the cytoplasmic end of the channel. The molecular determinants of charge selectivity, however, are unknown. We investigated the role of Arg352, a residue flanking the predicted cytoplasmic end of the M6 segment, in the mechanism of charge selectivity. We determined the Cl^- to Na^+ permeability ratio (P_{Cl}/P_{Na}) from the reversal potential measured in a 10-fold NaCl gradient. For the wild type, P_{Cl}/P_{Na} was 36 (range of 28−51). For the R352H mutant, P_{Cl}/P_{Na} was dependent on cytoplasmic pH. At pH 5.4, the P_{Cl}/P_{Na} was 33 (range of 27−41), similar to that of the wild type, but at pH 7.2, where the histidine should be largely uncharged, P_{Cl}/P_{Na} was 3 (range of 2.9−3.1). For the R352C and R352Q mutants, P_{Cl}/P_{Na} was 7 (range of 6−8) and 4 (range of 3.5−4.4), respectively. Furthermore, Na^+ which does not carry a significant fraction of the current through the wild type is measurably conducted through R352Q. Thus, the charge of the side chain at position 352 is a strong determinant of charge selectivity. In the wild type, the positive charge on Arg352 contributes to an electrostatic potential in the channel that forms a barrier to cation permeation. Mutation of Arg352 did not alter the halide selectivity sequence. Selectivity among halides must involve other residues.

The cystic fibrosis transmembrane conductance regulator (CFTR)[1] is a member of the ATP-binding-cassette membrane transporter gene superfamily. It forms a small-conductance, chloride channel that is gated by protein kinase A-mediated phosphorylation and by ATP binding and hydrolysis (*11*−*13*). The channel is lined, at least in part, by residues from the 12 putative membrane-spanning segments (Figure 1A) (*14*, *15*). The selectivity of the channel for anions over cations is likely to be a property of the channel-lining residues, but the key residues have not been identified. Mutation of four positively charged residues in membrane-spanning segments, Lys95, Lys335, Arg347, and Arg1030, to negatively charged residues did not alter the chloride to sodium permeability ratio (*7*).

Using the substituted-cysteine-accessibility method (*16*), we identified channel-lining residues in the M1, M3, and M6 (Figure 1B) membrane-spanning segments of CFTR (*17*−*19*). Cysteines substituted for 11 of 26 residues in and flanking the M6 membrane-spanning segment (residues 329−353) were accessible to charged, sulfhydryl-specific reagents which are derivatives of methanethiosulfonate (MTS) (*20*). We inferred that these MTS-reactive residues were on the water-accessible surface of the protein and that most of these residues line the channel (Figure 1B) (*19*). By comparing the ratio of the rates of reaction of negatively and positively charged derivatives of MTS with those of channel-lining, engineered cysteine residues in the M6 segment, we demonstrated that both anions and cations could enter the extracellular end of the channel and that both could penetrate to the level of Ser341 with no charge discrimination (*21*). Thus, the charge selectivity filter, the structure that discriminates between anions and cations, is located near the cytoplasmic end of the channel in the region of Thr351−Gln353 (Figure 1B) (*21*). We hypothesized that Arg352, the intervening residue, might be an important determinant of charge selectivity in the CFTR channel (*21*). Here we report the effects of mutating Arg352 on the charge selectivity, conductance, and halide selectivity of CFTR. The results support our hypothesis that Arg352 is a major determinant of charge selectivity in the CFTR channel.

EXPERIMENTAL PROCEDURES

Plasmids, Cell Culture, and Transfection. The *Kpn*I site in the CFTR-pCEP4 vector (*22*) was mutated to an *Nhe*I site by unique site elimination mutagenesis (*23*). A 4.6 kb cDNA encoding human CFTR was excised from the resulting plasmid by restriction digestion with *Nhe*I and *Xho*I and

† This work was supported by NIH Grants DK51794 and NS30808, the Cystic Fibrosis Foundation, a Grant-in-Aid from the New York City Affiliate of the American Heart Association, and a fellowship from the Fondation pour la Recherche Medicale (to R.G.). M.H.A. is an Established Scientist of the New York City Affiliate of the American Heart Association.

* To whom correspondence and reprint requests should be addressed: Center for Molecular Recognition, 630 W. 168th St., New York, NY 10032. Telephone: (212) 305-3974. Fax: (212) 305-5594. E-mail: ma14@columbia.edu.

‡ Center for Molecular Recognition.

§ Departments of Physiology & Cellular Biophysics and Medicine.

[1] Abbreviations: CFTR, cystic fibrosis transmembrane conductance regulator; E_{rev}, reversal potential; *I*/*V* curve, current−voltage curve; MTS, methanethiosulfonate; P_{Cl}/P_{Na}, Cl^- to Na^+ permeability ratio.

10.1021/bi990155n CCC: $18.00
Published on Web 04/03/1999

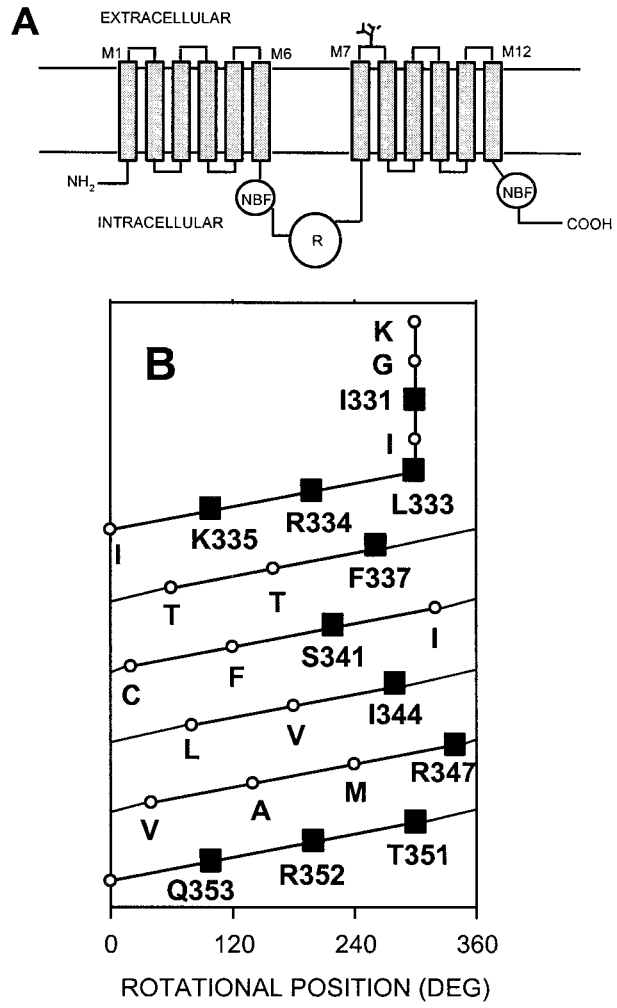

FIGURE 1: Predicted transmembrane topology of CFTR and the amino acid sequence in and flanking the M6 membrane-spanning segment. (A) The predicted transmembrane topology of CFTR (*14*). NBF is the nucleotide binding domain; R is the regulatory domain. (B) α-Helical net representation of the residues in and flanking the M6 membrane-spanning segment. The extracellular end is at the top; the intracellular end is at the bottom. The *x*-axis represents the position on the circumference of the helix. The residues that are aligned vertically lie on the same face of an ideal, α-helix. Black squares denote residues for which the corresponding cysteine substitution mutants were accessible to MTS reagents (*19*). Open circles denote residues for which the corresponding cysteine substitution mutants were unaffected by the MTS reagents. On the basis of hydrophobicity analysis, the M6 segment was predicted to extend from Gly330 to Val350 (*14*). Note that three consecutive residues flanking the cytoplasmic end of the M6 segment, Thr351, Arg352, and Gln353, are exposed in the channel (*19*). The secondary structure of these residues was inferred to be non-α-helical (*19*, *21*).

subcloned into a pCI-Neo vector (Invitrogen, Carlsbad, CA) modified to contain these restriction sites in the multiple cloning site.

CFTR mutants were generated as described previously (*19*) and subcloned into CFTR-pCI-Neo using a cassette defined by the restriction sites for *Acc*B7I and *Bsp*EI. The mutations and subcloning were confirmed by restriction digestion and DNA sequencing.

CHO cells were maintained in DMEM and 10% fetal calf serum at 37 °C with 5% CO_2. Cells (80% confluent), in 35 mm dishes, were cotransfected, 1 day after being split; 2 μg of the CFTR-pCI-Neo plasmid, 0.4 μg of a plasmid expressing green fluorescent protein (*24*) under a CMV promoter, and 9 μL of lipofectamine were mixed with OPTIMEM (GibcoBRL, Grand Island, NY) to a total volume of 1 mL, and the mixture was added to the cells. The cells were incubated for 6 h with the DNA/lipofectamine mixture before fresh medium was added.

Cells were used 1−3 days after transfection. Transfected cells were identified by the presence of green fluorescent protein and used for patch-clamp recording. CFTR-induced currents were detected in more than 90% of the green fluorescent cells. The wild type and all of the mutants were studied in cells from at least two separate transfections.

Electrophysiology. Single-channel and whole-cell currents were recorded under voltage clamp with an EPC9 HEKA patch-clamp amplifier controlled with Pulse 7.5 software for Power Macintosh (HEKA Electronik, Lambrecht, Germany). Currents were recorded through a PCM-2 A/D adapter (General Medical Systems, Greenville, NY) onto VCR tape. Data were subsequently played back and filtered (210 Hz) through a model 902LPF eight-pole Bessel filter (Frequency Devices, Inc., Haverhill, MA) and digitized using the Pulse software.

In the whole-cell experiments (*25*), the pipet contained 140 mM CsCl, 1.2 mM $MgCl_2$, 5 mM EGTA, 0.5 mM Na_2ATP, and 10 mM HEPES adjusted to pH 7.2 with CsOH. In most of the single-channel experiments (*25*), the pipet contained 140 mM NaCl, 4.8 mM KCl, 1.2 mM $MgCl_2$, 1 mM $CaCl_2$, and 10 mM HEPES adjusted to pH 7.2 with NaOH. When indicated in the text or figure legends, the pipet contained 145 mM *N*-methyl-D-glucamine (NMDG) chloride, 1.2 mM $MgCl_2$, 1 mM $CaCl_2$, and 10 mM HEPES adjusted to pH 7.4.

The bath solution was varied with the specific experiment. For recordings in symmetrical NaCl solutions, the bath contained 140 mM NaCl, 4.8 mM KCl, 1.2 mM $MgCl_2$, 2 mM EGTA, 0.5 mM Na_2ATP, and 10 mM HEPES adjusted to pH 7.2 with NaOH. To determine the Cl^- to Na^+ permeability ratio, a low-concentration NaCl bath solution was used to measure the reversal potential in a 10-fold NaCl gradient; this solution contained 14 mM NaCl, 1.2 mM $MgCl_2$, 2 mM EGTA, 0.5 mM Na_2ATP, 256 mM sucrose, and 10 mM HEPES adjusted to pH 7.2 with NaOH. MES buffer was substituted for HEPES when the pH of the bath solution was reduced to 5.4. To measure the permeability ratios with halides or gluconate, the NaCl in the bath was replaced with NaF, NaBr, NaI, or sodium gluconate at the same concentration.

The bath reference was 3 M KCl (in a 2% agar bridge) connected to a Ag−AgCl pellet. The applied potentials correspond to the difference between bath and pipet potentials, $V_{bath} - V_{pipet}$. The membrane potentials were corrected for the liquid junction potentials arising from changes in bathing solutions at the inner surface of the membrane patch. Variations in liquid junction potentials were measured with a pipet containing 2.7 M KCl by measuring the zero-current voltage deflection induced by the NaCl substitution solutions as described previously (*26*). All experiments were conducted at room temperature.

Prior to inside-out patches being obtained, CFTR channels were activated by incubating the cells for at least 10 min in 200 μM 8-(4-chlorophenylthio)adenosine cyclic monophosphate, 1 mM 3-isobutyl-1-methylxanthine, and 20 μM

forskolin (referred to as the cAMP-activating reagents). In the experiments in the cell-attached configuration designed to examine the extent and time course of channel activation, these reagents were added to the bath after obtaining the cell-attached patch.

Data Analysis. Single-channel records digitized with the Pulse software (HEKA Electronik) were analyzed using the Pulse 7.5 or TAC 2.5 software (Bruxton, Seattle, WA). The magnitudes of the single-channel currents were determined using the Pulse 7.5 program. For each voltage, the single-channel amplitudes of individual channel openings were determined using manually positioned cursors. If the baseline current immediately following a channel opening changed from the baseline current preceding the opening event by more than 10% of the amplitude of the opening, then the event was not used. For each patch, at each voltage, the average current amplitude was calculated from the magnitudes of several channel openings; the averages were used to determine the *I*/*V* relationship for the patch.

In symmetrical 140 mM NaCl for each patch, the single-channel conductance was determined from the slope of a linear regression fit of the single-channel current−voltage data. For each mutant, the reported conductances are averages from multiple patches.

In the presence of a 10-fold NaCl gradient, the reversal potential was determined for each patch by linear regression analysis. Only the data for positive current values were included in the linear regression fits. This was done because with the smaller number of charge carriers on the low-salt side the single-channel currents at potentials more negative than the reversal potential were small, often less than 0.2 pA, the level of the noise in our system. At potentials more negative than −100 mV, the patches became unstable; thus, we could only measure the single-channel currents at voltages significantly more negative than the reversal potential for mutants with reversal potentials close to zero. For the wild type and mutants with reversal potentials near −50 mV, the number of points at voltages more negative than the reversal potential were insufficient to perform a nonlinear regression analysis to determine the reversal potential; therefore, we used the linear regression of the positive currents to estimate the reversal potential. The reversal potential for each patch was determined by extrapolating the linear regression fit to the *x*-axis intercept. The reversal potentials obtained for multiple patches for a given mutant were averaged. The averaged reversal potential was used to calculate the Cl^- to Na^+ permeability ratio using the Goldman equation (*27*−*29*). To provide an estimate of the error in the Cl^- to Na^+ permeability ratio, we calculated the range of the Cl^- to Na^+ permeability ratio based on the standard error of the reversal potential.

In the figures containing *I*/*V* plots, the single-channel current amplitudes from multiple patches were averaged and the solid lines are fit to the averages by nonlinear regression analysis SigmaPlot 2.0 (Jandel Corp., Corte Madera, CA). Therefore, the *x*-intercept of the solid lines in the figures may be different from the reversal potential calculated as described above and given in the text.

RESULTS

Characterization of Wild-Type and Mutant CFTR Expression. Wild-type CFTR and the CFTR mutants were expressed in CHO cells by transient transfection. Functional CFTR channels were observed in patch clamp recordings 1−3 days after transfection. In cell-attached patches, with 140 mM NaCl in the pipet, the single-channel conductances (in picosiemens) were 6.0 ± 0.3 for the wild type ($n = 7$), 5.3 ± 0.3 for R352C ($n = 11$), 4.2 ± 0.1 for R352Q ($n = 10$), 4.0 ± 0.2 for R352H ($n = 4$), and 5.7 ± 0.2 for Q353C ($n = 8$). The current−voltage relationships (*I*/*V* curve) displayed slight outward rectification (data not shown) as observed in previous studies of CFTR expressed in CHO cells (*30*). No CFTR-like channels were observed in patches from mock-transfected cells stimulated with the cAMP-activating reagents ($n = 10$) as previously reported (*30*).

In cell-attached patches from unstimulated cells expressing wild-type CFTR, on average 1 ± 0.25 ($n = 12$) channel was observed, presumably activated by endogenous cAMP levels. In the same membrane patches after application of the cAMP-activating reagents, the number of open channels increased and reached a plateau within 1.9 ± 0.2 min, at which point a macroscopic current equivalent to 37 ± 15 ($n = 12$) open channels was observed. In cells expressing the R352C mutation, active channels were observed in about half of the cell-attached patches; 0.6 ± 0.3 ($n = 12$ patches) channel was observed before activation, and 4.9 ± 0.8 channels were observed after application of the cAMP-activating reagents. The time required to reach maximal activation was 3.7 ± 0.7 min ($n = 12$).

The relative magnitudes of the CFTR-induced currents observed in whole-cell recordings were consistent with the numbers of channels observed in cell-attached patches. The conductance of untransfected cells was 0.6 ± 0.03 nS ($n = 3$). Following activation with cAMP, cells transfected with wild-type CFTR had a conductance of 12 ± 2 nS ($n = 6$) and cells transfected with R352C had a conductance of 2 ± 0.3 nS ($n = 8$) (Figure 2A). We determined the Cl^- to Na^+ selectivity using single-channel current−voltage relationships because in whole-cell measurements the selectivity of the background conductance would have a different effect on the reversal potential measured for the wild type and the mutants due to the difference in the magnitude of the currents of the wild type and the mutants relative to the background current of the cell.

In inside-out patches, with symmetrical solutions containing 140 mM NaCl in the pipet and in the bath, the wild type and the mutants had linear current−voltage relationships and reversal potentials of 0 mV (Figure 2B−D). The single-channel conductances (in picosiemens) were 6.2 ± 0.5 for the wild type ($n = 6$)[2] (Figure 3B), 5.9 ± 0.3 for R352C ($n = 5$), 4.2 ± 0.1 for R352Q ($n = 8$), and 5.7 ± 0.3 for Q353C ($n = 8$). For the R352H mutant, the single-channel conductance was sensitive to the pH of the bath solution; the single-channel conductance at pH 7.2 was 3.7 ± 0.1 pS ($n = 6$), and at pH 5.4, it was 4.3 ± 0.1 pS ($n = 5$) (Figure 4). The single-channel conductance of the wild type at pH 5.4 was 5.5 ± 0.3 pS ($n = 5$) (data not shown), slightly smaller than the conductance that we measured at pH 7.2.

[2] The single-channel conductance that we observe is slightly smaller than that reported by other investigators. This may be due to the presence of HEPES buffer which causes a slight block of Cl^- channels (*1*−*3*). Because it is present symmetrically in both the pipet and bath solutions, it does not affect our conclusions.

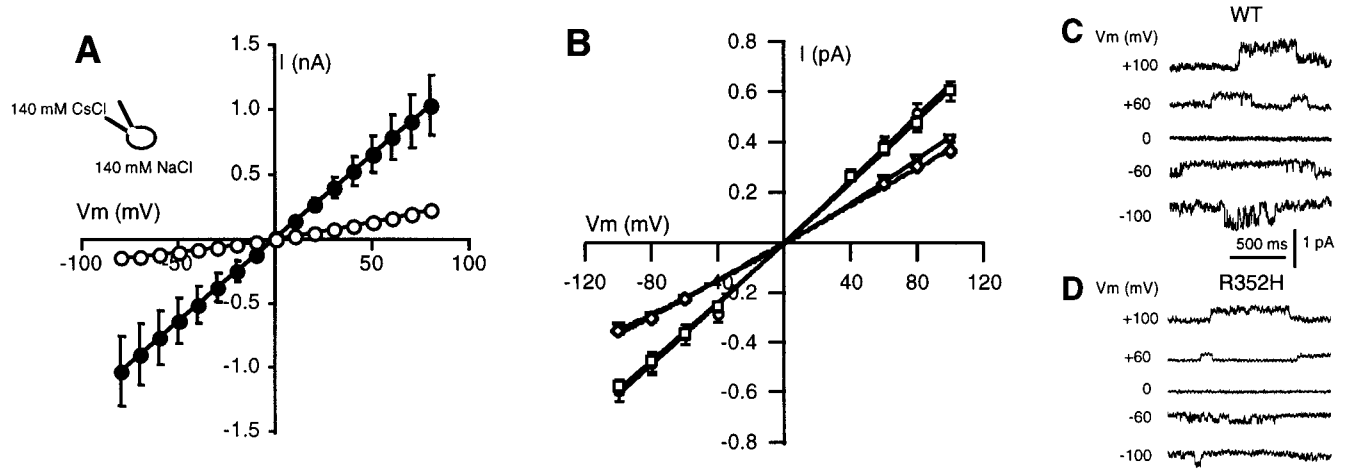

FIGURE 2: Whole-cell and single-channel current−voltage relationships for the wild type and Arg352 mutants in symmetrical Cl^--containing solutions. (A) Average whole-cell current−voltage relationships obtained from cells expressing either wild-type CFTR (●) or the R352C mutant (○) in symmetrical Cl^--containing solutions. Note the much lower level of current in the R352C mutant than in the wild type. (B) Average single-channel current−voltage relationships for the wild type (○) and the R352C (□), R352Q (▽), and R352H (bath pH of 7.2) (◇) mutants. The symbols for the wild type and R352C are indistinguishable at several voltages. The symbols for R352Q and R352H overlap at several voltages. The solid lines represent a fit by nonlinear regression analysis connecting the points. Error bars (standard error of the mean) are smaller than the symbols in some cases. (C and D) Single-channel recordings from inside-out patches obtained from cells expressing either (C) wild-type CFTR or (D) the R352H mutant (bath pH of 7.2). Holding potentials are indicated at the left of each trace. Recordings were filtered at 210 Hz.

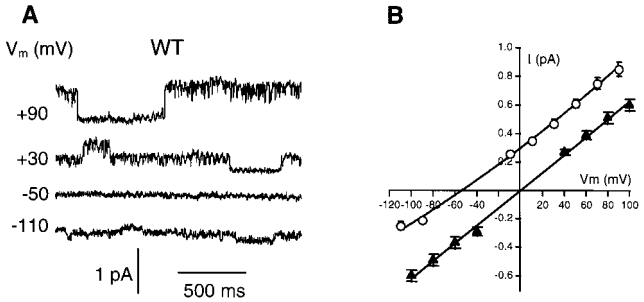

FIGURE 3: Wild-type CFTR forms highly anion-selective channels. (A) Single-channel currents from wild-type CFTR at different membrane voltages using the inside-out patch configuration in the presence of a 10-fold NaCl gradient. The pipet contained the standard 140 mM NaCl solution. The bath solution contained the low-NaCl solution (14 mM NaCl). Currents were filtered at 210 Hz. (B) Single-channel current−voltage relationship for wild-type CFTR. Black triangles depict the *I*/*V* curve obtained in symmetrical conditions where both sides of the membrane were bathed with 140 mM NaCl. Open circles depict the *I*/*V* curves obtained in the presence of a 10-fold NaCl gradient as described above (average of seven patches). The solid lines represent a fit by nonlinear regression analysis connecting the points for a given mutant, and therefore, the *x*-intercept may not correspond precisely to the actual reversal potentials calculated as described in Experimental Procedures. Error bars (standard error of the mean) are smaller than the symbols in some cases.

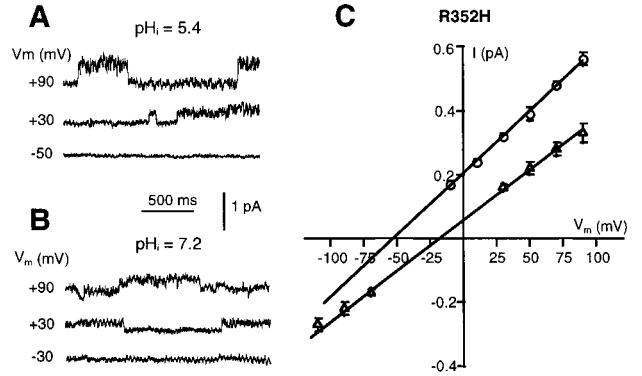

FIGURE 4: Reversal potential of the R352H mutant which is shifted by the protonation state of the histidine. Single-channel recordings for R352H at various applied voltages in a 10-fold NaCl gradient as described in Figure 3A except the bath pH was 5.4 (A) and 7.2 (B). (C) Single-channel current−voltage relationships for R352H with the bath pH at pH 5.4 (○) and pH 7.2 (△). The solid lines represent a fit by nonlinear regression analysis connecting the points for a given mutant, and therefore, the *x*-intercept does not correspond precisely to the actual reversal potentials calculated as described in Experimental Procedures. Note the shift in the reversal potential between pH 5.4 and 7.2, that is, between the protonated and unprotonated states of the histidine. Error bars (standard error of the mean) are smaller than the symbols in some cases.

Cl^- to Na^+ Permeability Ratio for Wild-Type CFTR. To determine the Cl^- to Na^+ permeability ratio of the wild type and the mutants, we measured the reversal potential of the single-channel currents in the presence of a 10-fold NaCl gradient. For each patch, the reversal potential (E_{rev}) was determined by extrapolation from a linear regression fit of the single-channel current−voltage data. As described in Experimental Procedures, for wild-type CFTR and all of the mutants, only the data obtained at positive currents were used for the linear regression fit.

For wild-type CFTR in a 10-fold NaCl gradient, E_{rev} was -51 ± 1.5 mV ($n = 7$) (Figure 3). Using the voltage Goldman−Hodgkin−Katz equation (*27*−*29*), the calculated Cl^- to Na^+ permeability ratio (P_{Cl}/P_{Na}) was 36 (range of 28−51). The reversal potential of the wild type was the same at pH 5.4, -50.3 ± 1.9 mV ($n = 4$), (data not shown) and at pH 7.2, indicating that in the wild type, in this pH range, charge selectivity exhibits no pH dependence.

The addition of sucrose to the cytoplasmic bath solution was reported to cause a flickery block of inward CFTR single-channel currents (i.e., outward Cl^- movement) (*31*). For wild-type CFTR in a 10-fold NaCl gradient without sucrose in the bath, the single-channel conductance was 5.8 $\pm$ 0.2 pS and the reversal potential E_{rev} was -50 ± 1.4 mV ($n = 6$), not significantly different from the reversal potential determined in the presence of sucrose (Figure 5). Similarly, for the R352Q mutant in the 10-fold NaCl gradient in the

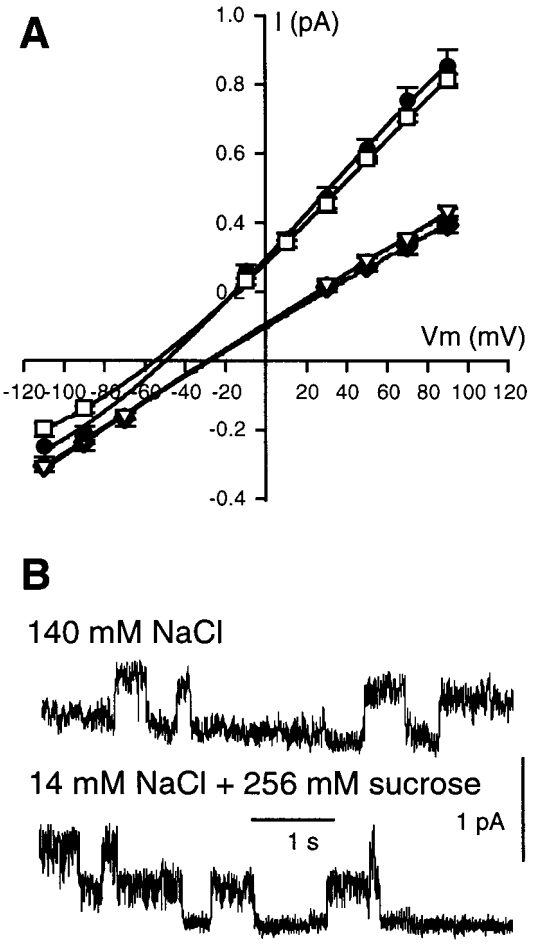

FIGURE 5: Sucrose in the cytoplasmic bath does not alter the reversal potentials determined from the outward currents for the wild type and the R352Q mutant. (A) Single-channel current−voltage relationships for the wild type (● and □) and the R352Q mutant (◆ and △) in the presence of the 10-fold NaCl gradient. The data depicted by the white symbols were obtained with no sucrose in the bath, and the data depicted by the black symbols were obtained with 256 mM sucrose in the bath. (B) Single-channel currents recorded from patches excised from different cells expressing wild-type CFTR. The top trace was recorded from a patch bathed by symmetrical 140 mM NaCl ($V_m = 60$ mV) and the lower trace from a patch with 140 mM NaCl in the pipet and 14 mM NaCl and 256 mM sucrose in the bath ($V_m = 30$ mV). Note that the reversal potentials and the conductances for the wild type and the R352Q mutant were not affected by the presence or absence of sucrose.

absence of sucrose in the cytoplasmic bath, the single-channel conductance was 3.8 ± 0.1 pS and the E_{rev} was −27.4 ± 1.2 mV ($n = 9$) (Figure 5), not significantly different from the values measured in the presence of sucrose (see below). Therefore, we included sucrose in the cytoplasmic bath solution to balance the osmolarity in the 10-fold NaCl gradient because we found that it improved the stability of the patches.

Cl^- to Na^+ Permeability Ratios of the Arg352 Mutants. To determine the role of the positive charge at position 352, we substituted histidine for Arg352. With the histidine mutant, we should be able to alter the charge at this position by changing the pH of the cytoplasmic bath. Maintaining the positive charge at position 352 with the R352H mutation and a bath pH of 5.4 gave a reversal potential E_{rev} of −50.4 ± 1.2 mV ($n = 7$) (Figure 4), which was not significantly different from that of the wild type. The calculated P_{Cl}/P_{Na} equaled 33 (range of 27−41), similar to that of the wild type. In contrast, removing the positive charge at position 352 by raising the pH of the cytoplasmic bath to 7.2 significantly reduced the reversal potential E_{rev} to −21.4 ± 0.6 mV ($n = 5$) at pH 7.2 (Figure 4), resulting in a calculated Cl^- to Na^+ permeability ratio of only 3 (range of 2.9−3.1).

We further tested the effect of removing the positive charge at position 352 by substituting the uncharged residues cysteine and glutamine at this position. These uncharged substitutions also shifted the reversal potential by an amount comparable to that observed by deprotonating R352H; $E_{rev} = -34.9 \pm 2$ mV ($n = 7$) for R352C, and $E_{rev} = -26.3 \pm 1.9$ mV ($n = 9$) for R352Q (Figure 6), resulting in calculated P_{Cl}/P_{Na} ratios of 7 (range of 6−8) and 4 (range of 3.5−4.4), respectively.

We substituted a negatively charged residue at position 352. Unfortunately, the single-channel conductance and kinetics of the R352E mutant appeared to be too small to accurately determine the reversal potential.

In the experiments described above, the reversal potential was measured in a 10-fold NaCl gradient. To be sure that the measured reversal potentials were not significantly affected by the low ionic strength of the cytoplasmic solution, we measured the reversal potentials for the wild type and R352Q following replacement of NaCl in the bath with sodium gluconate. For the wild type, no single-channel currents were observed at potentials more negative than the predicted reversal potential when the cytoplasmic Cl^- was replaced by gluconate, consistent with previous observations that gluconate is either poorly permeant or impermeant (Figure 7C, □) (*32*, *33*). For the R352Q mutant, we could not clearly identify single currents at potentials more negative than the reversal potential calculated by extrapolation from the currents seen at positive potentials. The reversal potential for R352Q calculated by extrapolation from the single-channel currents observed at positive potentials was −33.3 ± 1.4 mV ($n = 9$) (Figure 7D, □), close to that predicted with the Goldman−Hodgkin−Katz equation given the Cl^- to Na^+ permeability ratios calculated above in the 10-fold NaCl gradient and assuming that gluconate is impermeable through CFTR. Thus, the effects of the mutations on the Cl^- to Na^+ permeability ratios were not significantly affected by the low ionic strength of the cytoplasmic solution in the 10-fold NaCl gradient.

Mutation of the adjacent residue (Q353C) did not alter the reversal potential relative to that of the wild type [$E_{rev} = -51.1 \pm 1.7$ mV (n=7)], and thus, the Cl^- to Na^+ permeability ratio was the same as that of the wild type ($P_{Cl}/P_{Na} = 36$). This indicates that the glutamine is not involved in the mechanism of charge selectivity.

Effects of Arg352 Mutation on the Charge of Permeating Ions. The fractional current carried by a specific ion through the channel can be inferred from changes in conductance following ion substitutions.[3] Therefore, we measured the Cl^- to Na^+ conductance ratios in the wild type ($P_{Cl}/P_{Na} = 36$) and in the R352Q ($P_{Cl}/P_{Na} = 4$) mutant to determine whether Na^+ carries a significant fraction of the current in the mutants. To investigate this issue, we examined the effect on the single-channel currents of substituting *N*-methyl-D-glucamine ($NMDG^+$) for Na^+.

With wild-type CFTR in inside-out patches, as was reported previously (*9*), substituting NMDG-Cl for NaCl in

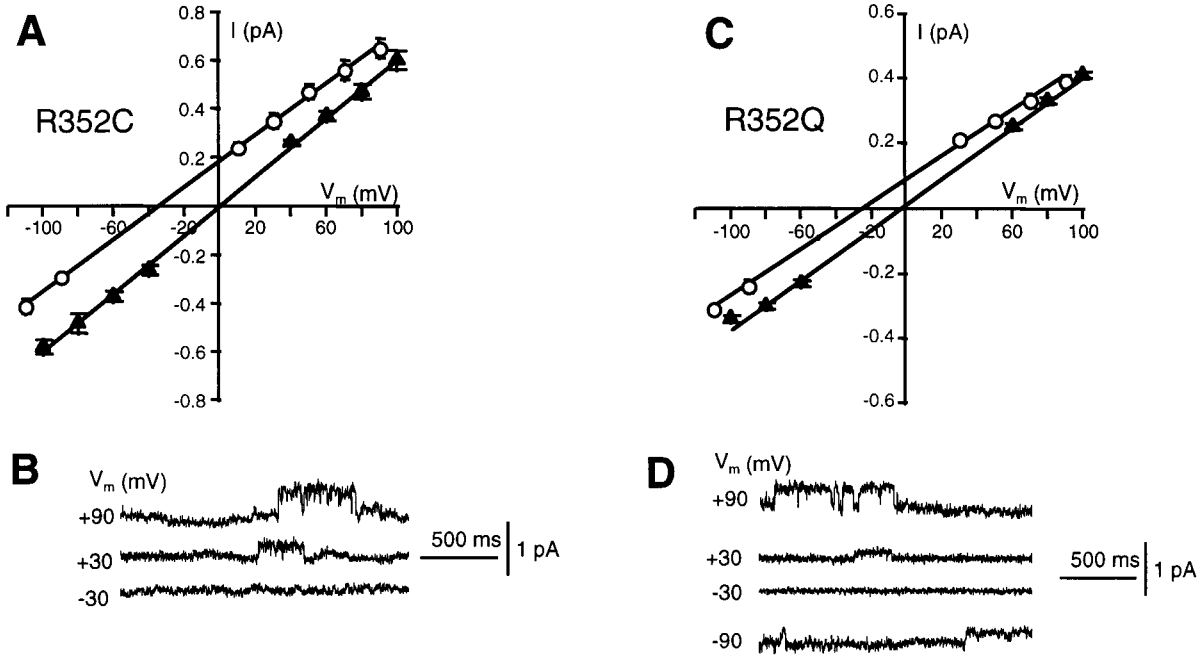

FIGURE 6: Substituting uncharged residues at position 352 reduces the anion to cation selectivity ratio. (A and C) Average single-channel current−voltage relationships for the R352C (A) and R352Q (C) mutants in symmetrical 140 mM NaCl (▲) and in the presence of the 10-fold NaCl gradient (○) as described in the legend of Figure 3A. The solid lines represent a fit by nonlinear regression analysis connecting the points for a given mutant, and therefore, the *x*-intercept does not correspond precisely to the actual reversal potentials determined as described in the Experimental Procedures. Error bars (standard error of the mean) are smaller than the symbols in some cases. (B and D) Single-channel recordings are shown for the R352C (B) and R352Q (D) mutants. The recordings were obtained in the presence of the 10-fold NaCl gradient as described in the legend of Figure 3A. The holding potential is shown to the left of each trace.

the bath does not alter the single-channel *I*/*V* relationship compared to the *I*/*V* relationship recorded in symmetrical NaCl (Figure 7C, ▲ vs ○). With NMDG-Cl in the bath, the single-channel conductance was 6 ± 0.3 pS and E_{rev} equaled 2.7 ± 0.9 mV (n = 10). Thus, Na^+ does not carry a significant fraction of the current through wild-type CFTR. In contrast, substitution of gluconate for Cl^- in the bath shifted the *I*/*V* relationship toward negative voltages, and no single-channel currents were observed at potentials more negative than the predicted reversal potential. The single-channel conductance in the positive potential range was 5.4 ± 0.2 pS (n = 6) (Figure 7B,C, □ vs ▲). The slight reduction in the single-channel conductance may be due to the rapid flickery block induced by the cytoplasmic gluconate as previously reported (*31*). These results are consistent with previous reports (*7*, *9*, *32*, *33*) and indicate that for wild-type CFTR gluconate, Na^+ and $NMDG^+$ are not measurably permeable at the single-channel level and that Cl^- is the major charge carrier of current through the channel.

In R352Q, the effects of substituting $NMDG^+$ for Na^+ were different than in the wild type. For the R352Q mutant, in inside-out patches, substituting NMDG-Cl for NaCl in the bath changed the current−voltage relationship from linear in symmetrical NaCl to inwardly rectifying (Figure 7D, ▲ vs ○) and caused the reversal potential to shift to 8.6 ± 0.8 mV (n = 8). The outward single-channel conductance, i.e., when $NMDG^+$ in the bath and Cl^- in the pipet would be moving through the channel, was reduced to 3.1 ± 0.1 pS while the inward conductance remained 4.2 ± 0.1 pS (n = 8). This indicates that Na^+ was carrying about 25% of the current in this mutant. When sodium gluconate was substituted for NaCl in the bath, the reversal potential E_{rev} shifted to −33.3 ± 1.4 mV and the outward single-channel conductance remained 4.1 ± 0.2 pS. Thus, for the R352Q mutant, the conductance of Cl^- is about 3 pS and the conductance of Na^+ is about 1 pS, giving a Cl^- to Na^+ conductance ratio of 3, similar to the permeability ratio of 4 for this mutant.

Effects of Arg352 Mutation on Halide Selectivity Ratios. To investigate whether Arg352 is also a determinant of the monovalent halide selectivity sequence, we measured the bi-ionic reversal potentials in the inside-out patch configuration when the bath Cl^- was replaced with various halide anions. For the wild type, we observed the permeability sequence that was previously reported: $Br^- > Cl^- > I^- > F^-$ (*7*−*10*).[4] The E_{rev} values of the *I*/*V* curves are 8 ± 1 mV (n = 6) for Br^-, −8 ± 1 mV (n = 8) for I^-, and −32 ± 3 mV (n = 6) for F^-. Similar reversal potentials were observed for the R352C mutant: 7 ± 1 mV (n = 8) for Br^-, −13 ± 1 mV (n = 6) for I^-, and −27 ± 2 mV (n = 5) for F^-. The calculated permeability ratios between these halides and chloride are given in Table 1. The similarity between the halide permeability ratios indicates that Arg352 is not a major determinant of the halide selectivity sequence.

[3] Permeability and conductance ratios assay different aspects of ion permeation through a channel. The reversal potentials used to calculate the permeability ratios are made under conditions of zero net current, whereas conductance ratios are determined under conditions of net flux and are thus more affected by the relative affinities of binding sites within the channel for the ions. Attempts to relate these ratios to energy profiles within a channel have been successful for simple models of ion channels, such as single-ion occupancy with a single rate-limiting barrier to ion permeation (*4*). Evidence, however, indicates that CFTR is a multiple-ion occupancy channel (*5*, *6*). In multiple-ion occupancy models, the relationship between permeability and conductance ratios and their relationship to the depths of wells and heights of barriers is model-dependent (*4*).

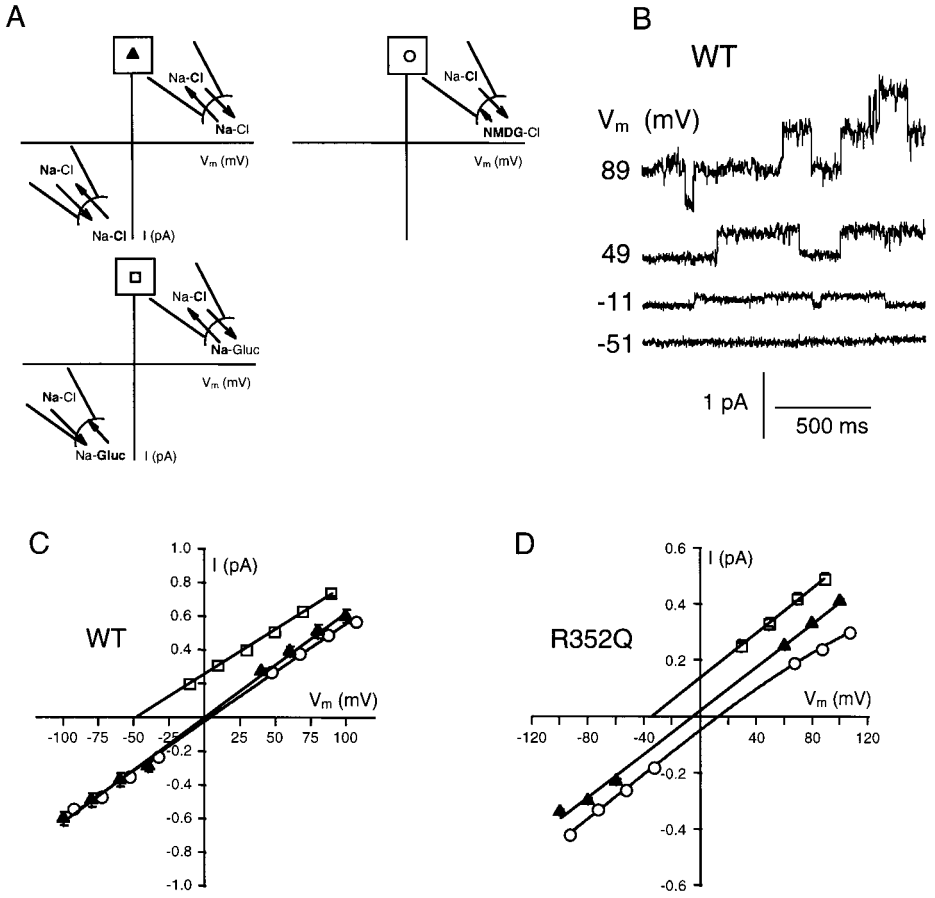

FIGURE 7: A fraction of the current is carried by Na^+ in the R352Q mutant but not in the wild type. (A) Cartoon illustrating the ion substitutions and the direction of ion movement in the positive and negative voltage ranges represented by the symbols in panels C and D. (B) Single-channel recordings from a patch containing wild-type CFTR with 140 mM NaCl in the pipet and 140 mM sodium gluconate in the bath. The holding potential is shown to the left of each trace. (C) Single-channel current−voltage relationships for wild-type CFTR under different ion gradients. The major salt in the pipet and in the bath are as illustrated in panel A (pipet/bath): NaCl/NaCl (▲), NaCl/NMDG-Cl (○), and NaCl/sodium gluconate (□). (D) Single-channel current−voltage relationships for R352Q under the same ion gradients. Symbols are like those in panel C. The solid lines represent a fit by nonlinear regression analysis connecting the points for a given mutant, and therefore, the *x*-intercept does not correspond precisely to the actual reversal potentials. Error bars (standard error of the mean) are smaller than the symbols in some cases. Note the decreased current at positive potentials when $NMDG^+$ replaces Na^+ in the bath for the R352Q mutant (○ vs ▲), whereas there is no effect of this substitution for the wild type.

For the wild type, the single-channel conductances were similar if the bath contained Cl^-, Br^-, or F^- (6.2 ± 0.5, 6.5 ± 0.5, and 5.8 ± 0.2 pS, respectively), whereas when the bath contained I^-, the single-channel conductance fell to 3.8 ± 0.2 pS (data not shown). Thus, unlike in a previous study (*34*), we observed that I^- was able to carry current through CFTR and that the I^- to Cl^- permeability ratio was similar to that observed when extracellular Cl^- was replaced by I^- (*7*−*10*). For the R352C mutant, the conductances were similar to that of the wild type (5.9 ± 0.3 pS for Cl^-, 5.2 ± 0.3 pS for Br^-, 5.7 ± 0.2 pS for F^-, and 3.6 ± 0.2 pS for I^-). The mechanism for the decreased I^- conductance compared to those of the other halide ions for both WT and R352C is not known, although in the R347D mutant the effect is eliminated (*2*).

Table 1: Halide Permeability Ratios (P_X/P_{Cl})[a]

	bromide	chloride	iodide	fluoride
wild type	1.39 ± 0.05	1	0.71 ± 0.02	0.25 ± 0.04
R352C	1.04 ± 0.04	1	0.54 ± 0.05	0.22 ± 0.03

[a] Permeability ratios for the halides relative to those for Cl^- for the wild type (WT) and the R352C mutant. Values (mean ± standard error of the mean) were calculated using the Goldman−Hodgkin−Katz equation for each experiment. Each value is the mean of at least five patches.

DISCUSSION

CFTR forms a highly anion-selective channel. Removing the positive charge at the position of Arg352 reduced the ability of the channel to discriminate between anions and cations as measured by both permeability and conductance ratios (Figures 3, 4, 6, and 7). In the R352H mutant, at a cytoplasmic pH of 5.4 when the histidine is mostly protonated, $P_{Cl}/P_{Na} = 33$, similar to that of the wild type. In contrast, at pH 7.2, when the histidine is mostly uncharged, $P_{Cl}/P_{Na} = 3$ (Figure 4C). A similar change in cytoplasmic

[4] For CFTR, the value of the I^- to Cl^- permeability ratio depends on whether the measurement of the reversal potential is taken immediately after the I^--containing solution is perfused into the bath or several minutes later (*2*). If the measurement is taken immediately after the I^- enters the bath, a high I^- to Cl^- permeability ratio is obtained (*2*); if the measurement is taken several minutes later, a low I^- to Cl^- permeability ratio is obtained (*2*, *7*−*10*). This I^--induced change appears to result from I^- binding to the CFTR protein and is eliminated by the R347D mutation (*2*). Our measurements were taken several minutes after the solution change, and thus, we obtained a low I^- to Cl^- permeability ratio.

pH did not alter P_{Cl}/P_{Na} for wild-type CFTR. Thus, for the R352H mutant, we infer that the effect of the change in cytoplasmic pH on the Cl^- to Na^+ permeability ratio is due to a change in the protonation state of the histidine at position 352.[5] Similarly, eliminating the positive charge at position 352 by substituting the uncharged amino acids, cysteine or glutamine, reduced P_{Cl}/P_{Na} to about 5 (Figure 6). Thus, substituting three different uncharged residues at position 352 reduced P_{Cl}/P_{Na} between 6- and 10-fold. In addition, the charge at position 352 is also a major determinant of the Cl^- to Na^+ conductance ratio,[3] that is, the fraction of the current that is carried by Cl^- vs Na^+. In wild-type channels, Na^+ does not carry a significant fraction of the current; thus, substituting $NMDG^+$ for Na^+ did not alter the current−voltage relationship as was previously shown (*8*, *9*). In contrast, in the R352Q mutant, substitution of $NMDG^+$ for Na^+ caused rectification of the current−voltage relationship due to a unidirectional elimination of the contribution of Na^+ to the single-channel conductance. Thus, in the mutants with a decreased Cl^- to Na^+ permeability ratio, Na^+ carries a measurable fraction of the current. Therefore, we infer that the charge at position 352 is a major determinant of charge selectivity in the CFTR channel.

Although the changes in permeability and conductance resulting from mutation of Arg352 are consistent with a direct effect of the charge at this position on the selectivity of the channel, we cannot exclude the possibility that the changes result from nonlocal perturbations of the protein structure. We do know, however, that Arg352 is in the channel lining because a cysteine substituted for Arg352 reacted with charged, sulfhydryl-specific MTS reagents (*19*) and the reaction rates were voltage-dependent (*21*). In addition, we previously showed that the process of charge selectivity occurs near the cytoplasmic end of the channel by measuring the relative reaction rates of negatively and positively charged MTS reagents with identified channel-lining residues in the M6 membrane-spanning segment (*21*). Our present results, based on an independent set of experiments, demonstrate that Arg352, flanking the cytoplasmic end of the M6 segment, is a major determinant of charge selectivity. This provides support for our previous inference regarding the location of the charge selectivity filter and confirmation of the approach to identifying the location of charge selectivity filters (*21*).

Other residues must also contribute, albeit to a lesser extent, to the process of charge selectivity, because the channel is still slightly anion-selective when uncharged residues are substituted at position 352. The identity of these other residues is at present unknown. P_{Cl}/P_{Na} was not effected by mutations of other positively charged residues in membrane-spanning segments, including Arg347 (M6) (*2*, *7*), Lys95 (M1), Lys335 (M6), and Arg1030 (M10) (*7*).

Model for Charge Selectivity. We hypothesize that charge selectivity in the CFTR channel results, at least in part, from an electrostatic interaction between fixed charges in the channel lining and ions in solution. In the wild-type channel, we infer that the positive charge on Arg352 creates a positive electrostatic potential in the channel lumen. This potential forms a barrier to cation movement through the channel. The effect of this potential appears to be greater on cations than on anions because substitution of glutamine for arginine increased the Na^+ conductance from an immeasurably low level in the wild type to about 1 pS in R352Q, whereas it only lowered the Cl^- conductance by about 50%, i.e., from 6 to 3 pS (Figure 7). It was suggested that a high-affinity chloride binding site, such as that found in the crystal structure of cartilage oligomeric matrix protein (*35*), might form the basis for charge selectivity in anion-selective channels. This is unlikely to be the mechanism in CFTR because Arg352 does not appear to form a high-affinity Cl^- binding site because the mutation R352C does not alter the halide selectivity sequence.

For Arg352 to function as the major determinant of charge selectivity, the channel lumen must be relatively narrow in the region of Arg352, thereby forcing ions to interact with its electrostatic potential as they attempt to move through this region of the channel. This narrow segment of the channel must extend over a relatively short distance, because mutation of Arg347, a channel-lining residue only five residues away in the linear sequence, does not alter P_{Cl}/P_{Na} (*2*, *7*). This suggests that the lumen might be significantly wider at the level of Arg347. Alternatively, other residues in close proximity to Arg347 may reduce its electrostatic contribution to the potential in the channel lumen. Similarly, Lys95 and Lys335, near the extracellular ends of the membrane-spanning segments, are not likely to be in the narrow portion of the channel, because mutation of these residues to anionic amino acids did not alter P_{Cl}/P_{Na} (*7*).

The minimum functional pore diameter of CFTR was inferred to be about 5.3 Å on the basis of the relative permeabilities of a series of progressively larger anions (*32*); however, more recent measurements suggest that the channel is measurably permeant to anions with diameters as large as 10−12 Å (*33*). The ability of the sulfhydryl-reactive MTS reagents to react with a cysteine substituted at position 352 implies that the diameter from the extracellular end to the level of Cys352 must be at least 6 Å, the smallest dimension of the MTS reagents (*19*). Thus, in the region of Arg352, the channel may narrow to a diameter of about 10−12 Å, but the channel diameter is likely to be larger over the rest of its length.

In the ClC Cl^- channel family, a highly conserved sequence, GKxGPxxH, appears to line the pore (*36*). Cysteines substituted for the Lys, Pro, and His residues in this sequence were accessible to MTS reagents (*36*). Mutation of the conserved Lys residue to glutamate caused a 6-fold reduction in anion selectivity (*36*). Thus, in both CFTR and ClC channels, positively charged amino acids in the channel lining of the narrow region of the pore contribute to the charge selectivity process.

Interactions between Arg352 and Various Permeating Anions. Mutation of Arg352 did not alter the halide perme-

[5] It is important to recognize that other properties of the CFTR channel are dependent on cytoplasmic pH. For example, in the wild type the single-channel conductance is 11% lower at pH 5.4 than at pH 7.2. This presumably results from a change in the protonation state of residues that are accessible to the cytoplasmic surface of the protein; however, these pH-dependent changes in the wild type do not alter the Cl^- to Na^+ permeability ratio. In contrast, in the R352H mutant raising the pH, presumably deprotonating His352, caused a 10-fold reduction in the Cl^- to Na^+ permeability ratio. The fact that substituting other uncharged residues, glutamine and cysteine, at position 352 caused similar changes in the Cl^- to Na^+ permeability ratio supports our inference that raising the bath pH reduces the charge selectivity of R352H by deprotonation of the histidine at position 352.

ability sequence. Thus, Arg352 is not likely to be a major anion binding site within the channel. Mutation to anionic residues of two positively charged residues, Lys95 and Lys335, near the extracellular ends of the M1 and M6 membrane-spanning segments altered the halide permeability ratios (*7*). Both residues are on the water-accessible surface of the protein (*18*, *19*). The mutation P99L also changed the halide permeability ratios (*37*); however, this is presumably due to effects of the mutation on protein conformation because this residue is not on the water-accessible surface of the protein (*18*, *19*). The mechanism(s) by which mutations change the halide permeability sequence is uncertain. The halide permeability ratios may result from interactions with multiple sites within the channel, and therefore, the effects of mutations at any individual site may not cause dramatic changes in the ratios (*38*).

Effects of the Arg352 Mutations on Single-Channel Conductance. In addition to altering the charge selectivity of the CFTR channel, some of the Arg352 mutations also altered the single-channel conductance. The mechanism by which these mutations alter the single-channel conductance has not been identified. Given that the mutations change the type of ion that carries the current, it is not surprising that the conductance may also be altered. Some of the mutations may also affect the gating kinetics, but we did not investigate these changes in this study. If a mutation induced rapid flickering of the channel, then because the recordings were filtered at 210 Hz the rapid flickering would be manifested as a reduced single-channel size. None of the mutations appeared to cause a voltage-dependent rapid flickering because all of the mutants have linear single-channel current−voltage relationships in symmetrical NaCl solutions. Thus, if one of the mutations induced a rapid flickering state, it is not voltage-dependent and therefore would not affect the reversal potential in the 10-fold NaCl gradient. A number of mutations both in membrane-spanning segments and in putative cytoplasmic domains have been shown to alter single-channel conductance and gating kinetics (*37*, *39*−*41*). In the absence of a high-resolution, three-dimensional structure for the channel, it is difficult, however, to determine the structural basis for these changes in functional properties of the channel.

Summary. In summary, we have shown that the residue at position 352 is a major determinant of charge selectivity in the CFTR channel. With a positively charged amino acid at this position, the channel is highly anion-selective, whereas with an uncharged residue, the channel is slightly anion-selective. We hypothesize that for the residue at this position to exert such an effect the channel diameter must be small in the region of Arg352, approximately 10−12 Å in diameter. This narrow region of the channel lumen must extend over a relatively short distance because mutations of Arg347, only five residues away in the linear sequence, have no effect on the Cl^- to Na^+ permeability ratio. We infer that the positive charge on Arg352 contributes to a positive electrostatic potential in the channel lumen that creates a barrier to cation permeation through the channel.

ACKNOWLEDGMENT

We thank Drs. Pamela Davis and Mitchell Drumm for the gift of the CFTR-pCEP4 plasmid, Tom Livelli for the green fluorescent protein plasmid, and Drs. Min Cheung, Jonathan Javitch, and Arthur Karlin for helpful discussions and comments on the manuscript.

REFERENCES

1. Hanrahan, J. W., and Tabcharani, J. A. (1990) *J. Membr. Biol. 116*, 65−77.
2. Tabcharani, J. A., Linsdell, P., and Hanrahan, J. W. (1997) *J. Gen. Physiol. 110*, 341−354.
3. Yamamoto, D., and Suzuki, N. (1987) *Proc. R. Soc. London, Ser. B 230*, 93−100.
4. Eisenman, G., and Horn, R. (1983) *J. Membr. Biol. 76*, 197−225.
5. Tabcharani, J. A., Rommens, J. M., Hou, Y. X., Chang, X. B., Tsui, L. C., Riordan, J. R., and Hanrahan, J. W. (1993) *Nature 366*, 79−82.
6. Linsdell, P., Tabcharani, J. A., and Hanrahan, J. W. (1997) *J. Gen. Physiol. 110*, 365−377.
7. Anderson, M. P., Gregory, R. J., Thompson, S., Souza, D. W., Paul, S., Mulligan, R. C., Smith, A. E., and Welsh, M. J. (1991) *Science 253*, 202−205.
8. Bear, C. E., Duguay, F., Naismith, A. L., Kartner, N., Hanrahan, J. W., and Riordan, J. R. (1991) *J. Biol. Chem. 266*, 19142−19145.
9. Kartner, N., Hanrahan, J. W., Jensen, T. J., Naismith, A. L., Sun, S., Ackerley, C. A., Reyes, E. F., Tsui, L.-C., Rommens, J. M., Bear, C. E., and Riordan, J. R. (1991) *Cell 64*, 681−691.
10. Cunningham, S. A., Worrell, R. T., Benos, D. J., and Frizzell, R. A. (1992) *Am. J. Physiol. 262*, C783−C788.
11. Riordan, J. R. (1993) *Annu. Rev. Physiol. 55*, 609−630.
12. Welsh, M. J., and Smith, A. E. (1993) *Cell 73*, 1251−1254.
13. Gadsby, D. C., Nagel, G., and Hwang, T.-C. (1995) *Annu. Rev. Physiol. 57*, 387−416.
14. Riordan, J. R., Rommens, J. M., Kerem, B. S., Alon, N., Rozmahel, R., Grzelczak, Z., Zielenski, J., Lok, S., Plavsic, N., Chou, J. L., Drumm, M. T., Iannuzzi, M. C., Collins, F. S., and Tsui, L. C. (1989) *Science 254*, 1066−1073.
15. Chang, X. B., Hou, Y. X., Jensen, T. J., and Riordan, J. R. (1994) *J. Biol. Chem. 269*, 18572−18575.
16. Akabas, M. H., Stauffer, D. A., Xu, M., and Karlin, A. (1992) *Science 258*, 307−310.
17. Akabas, M. H. (1998) *Biochemistry 37*, 12233−12240.
18. Akabas, M. H., Kaufmann, C., Cook, T. A., and Archdeacon, P. (1994) *J. Biol. Chem. 269*, 14865−14868.
19. Cheung, M., and Akabas, M. H. (1996) *Biophys. J. 70*, 2688−2695.
20. Stauffer, D. A., and Karlin, A. (1994) *Biochemistry 33*, 6840−6849.
21. Cheung, M., and Akabas, M. H. (1997) *J. Gen. Physiol. 109*, 289−300.
22. Xie, J., Drumm, M. L., Ma, J., and Davis, P. B. (1995) *J. Biol. Chem. 270*, 28048−28091.
23. Deng, W. P., and Nickoloff, J. A. (1992) *Anal. Biochem. 200*, 81−88.
24. Chalfie, M., Tu, Y., Euskirchen, G., Ward, W. W., and Prasher, D. C. (1994) *Science 263*, 802−805.
25. Hamill, O. P., Marty, A., Neher, E., Sakmann, B., and Sigworth, F. J. (1981) *Pfluegers Arch. 391*, 85−100.
26. Guinamard, R., Chraibi, A., and Teulon, J. (1995) *J. Physiol. (London) 485*, 97−112.
27. Goldman, D. E. (1943) *J. Gen. Physiol. 27*, 37−60.
28. Hodgkin, A. L., and Katz, B. (1949) *J. Physiol. (London) 108*, 37−77.
29. Hille, B. (1992) *Ionic Channels of Excitable Membranes*, 2nd ed., Sinauer Associates, Inc., Sunderland, MA.
30. Tabcharani, J. A., Chang, X. B., Riordan, J. R., and Hanrahan, J. W. (1991) *Nature 352*, 628−631.

31. Linsdell, P., and Hanrahan, J. W. (1996) *Am. J. Physiol. 271*, C628−C634.
32. Linsdell, P., Tabcharani, J. A., Rommens, J. M., Hou, Y. X., Chang, X. B., Tsui, L. C., Riordan, J. R., and Hanrahan, J. W. (1997) *J. Gen. Physiol. 110*, 355−364.
33. Linsdell, P., and Hanrahan, J. W. (1998) *J. Gen. Physiol. 111*, 601−614.
34. Tabcharani, J. A., Chang, X.-B., Riordan, J. R., and Hanrahan, J. W. (1992) *Biophys. J. 62*, 1−4.
35. Malashkevich, V. N., Kammerer, R. A., Efimov, V. P., Schulthess, T., and Engel, J. (1996) *Science 274*, 761−765.
36. Fahlke, C., Yu, H. T., Beck, C. L., Rhodes, T. H., and George, A. L., Jr. (1997) *Nature 390*, 529−532.
37. Sheppard, D. N., Travis, S. M., Ishihara, H., and Welsh, M. J. (1996) *J. Biol. Chem. 271*, 14995−15001.
38. Mansoura, M. K., Smith, S. S., Choi, A. D., Richards, N. W., Strong, T. V., Drumm, M. L., Collins, F. S., and Dawson, D. C. (1998) *Biophys. J. 74*, 1320−1332.
39. Seibert, F. S., Jia, Y., Mathews, C. J., Hanrahan, J. W., Riordan, J. R., Loo, T. W., and Clarke, D. M. (1997) *Biochemistry 36*, 11966−11974.
40. Sheppard, D. N., Rich, D. P., Ostedgaard, L. S., Gregory, R. J., Smith, A. E., and Welsh, M. J. (1993) *Nature 362*, 160−164.
41. Drumm, M. L., Wilkinson, D. J., Smit, L. S., Worrell, R. T., Strong, T. V., Frizzell, R. A., Dawson, D. C., and Collins, F. S. (1991) *Science 254*, 1797−1799.

BI990155N